Acoustic Vibrations of Metal−Dielectric Core−Shell Nanoparticles

ARTICLE *in* NANO LETTERS · JUNE 2011

Impact Factor: 13.59 · DOI: 10.1021/nl201672k · Source: PubMed

NANO LETTERS

LETTER

pubs.acs.org/NanoLett

Acoustic Vibrations of Metal-Dielectric Core−Shell Nanoparticles

Denis Mongin, Vincent Juvé, Paolo Maioli,* Aurélien Crut, Natalia Del Fatti, and Fabrice Vallée

FemtoNanoOptics group, LASIM, Université Lyon 1-CNRS, 43 Bd du 11 Novembre, 69622 Villeurbanne, France

Ana Sánchez-Iglesias, Isabel Pastoriza-Santos, and Luis M. Liz-Marzán

Departamento de Quimica Fisica and Unidad Asociada CISC, Universidade de Vigo, 36310 Vigo, Spain

Supporting Information

ABSTRACT: The acoustic vibrations of metal nanoparticles encapsulated in a dielectric shell ($Ag@SiO_2$) were investigated using a time-resolved femtosecond technique. The measured vibration periods significantly differ from those predicted for the bare metal cores and, depending on the relative core and shell sizes, were found to be either larger or smaller than them. These results show that the vibration of the whole core−shell particle is excited and detected. Moreover, vibrational periods are in excellent agreement with the predictions of a model based on continuum thermoelasticity. However, such agreement is obtained only if a good mechanical contact of the metal and dielectric parts of the core−shell particle is assumed, providing a unique way to probe this contact in multimaterial or hybrid nano-objects.

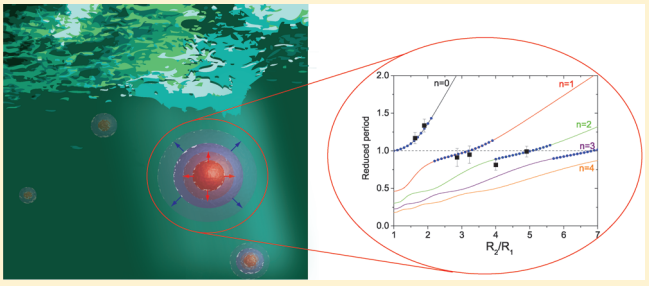

KEYWORDS: Core-shell nano-objects, silver nanoparticles, thermoelasticity, acoustic vibration modes, time-resolved spectroscopy

The possibility of designing and mastering the properties of nanostructured materials has led to considerable interest and activities in the academic and industrial domains. In this context, hybrid nano-objects (or nanohybrids) formed by two or more material components of different nature offer a wide range of possibilities for developing novel nanosystems. Proper design of nanohybrids should permit to control interaction of their components to combine different confinement-induced properties, create new ones, or introduce new functionalization or addressing possibilities. Key effects are here the electromagnetic, electrical, mechanical, or thermal coupling of their components. This is in particular the case in the optical domain for metal-based nanohybrids, for example, formed by a metal and a dielectric or semiconductor part.[1−6] In these systems, the plasmonic effect associated to the metallic part can be modified by the other component and/or exploited to enhance the overall optical response of the nanohybrids. This opens applications in many fields such as optomechanics,[7] biological imaging,[8] or medicine.[9,10]

The dependence of the properties of nano-objects on their characteristics can also be used as a tool for characterizing them, although this becomes a major challenge when they are composed of multiple materials. This approach, based on comparing their measured and computed responses, has been used on ensembles and single nano-objects by investigating their optical spectra.[11−13] However, for an electromagnetic coupling with a weak interaction of the optical excitations of the material components, optical measurements are only weakly sensitive to the details of the interface such as the local contact of the constituting materials. In this context, although they have been less exploited up to now, methods involving strong interface coupling are very interesting as they are sensitive to different length scales and should bring complementary information. This is the case of mechanical methods based on the study of the acoustic responses of nano-objects, which can now be readily investigated using noncontact spectrally or temporally resolved optical techniques (provided the nano-objects are located in a transparent matrix). The application of such approaches to nano-objects formed by a single material or two materials of the same nature (e.g., bimetallic) has shown that the frequency and damping of their vibrational modes contain information on both their morphology,[14−19] the structure and composition[20−23] and their mechanical contact with their environment.[24] Less results have been obtained in nanohybrids, where only fully decoupled vibrations of the shell of dielectric-metal core−shell nanospheres have been observed[25,26] (as also reported in Ni−Ag particles[27]).

To analyze the impact of interfacing and of the interfacial contact on the vibrational modes of nanohybrids, we have investigated model systems formed by metal-dielectric core−shell ($Ag@SiO_2$) nanospheres. Measurements were performed using time-resolved spectroscopy, which permits addressing the vibration of nano-objects in a very large size range.[14−16,26] Samples with various core diameters (in the 14−45 nm range) and shell thicknesses (in the 14−28 nm range) were synthesized. The results were found to be in excellent agreement with the predictions of a theoretical model based on continuum mechanics and taking

Received: May 18, 2011
Published: June 21, 2011

dx.doi.org/10.1021/nl201672k | *Nano Lett.* 2011, 11, 3016–3021

Table 1. Mean Core Radius (R_1) and Shell Thickness ($R_2 - R_1$) of the Investigated Ag@SiO_2 Samples

sample number	core radius R_1 (nm)	shell thickness R_2 - R_1 (nm)	R_2/R_1
1	22.5 ± 6.7	14.0 ± 2.0	1.6
2	15.6 ± 3.7	14.0 ± 1.6	1.9
3	8.4 ± 0.8	15.6 ± 1.0	2.9
4	6.5 ± 0.8	14.6 ± 1.1	3.2
5	7.0 ± 1.1	21.1 ± 1.1	4
6	7.0 ± 1.1	27.5 ± 2.0	4.9

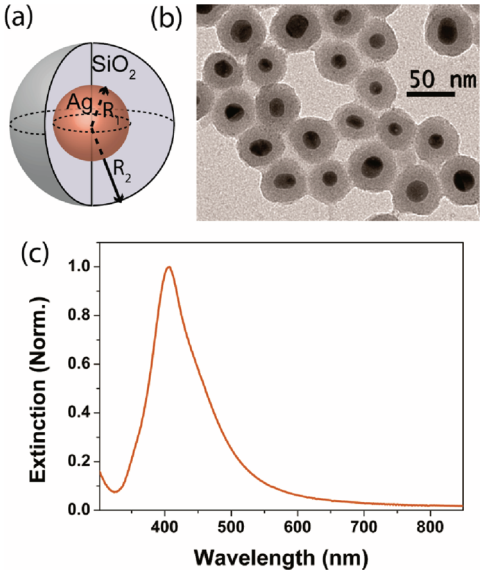

Figure 1. (a) Geometry of the Ag@SiO_2 nanoparticles formed by a silver core of radius R_1 and a silica shell of thickness $R_2 - R_1$. (b) Transmission electron microscopy image and (c) extinction spectrum of Ag@SiO_2 nanoparticles from sample 4.

into account mode selection due to the excitation and detection processes,[28] provided that a good mechanical contact between the core and shell material is assumed.

The preparation of Ag nanoparticles with various core radius, R_1 (see Table 1) was undertaken using different wet chemical methods, all previously reported[29−31] (more details about the synthesis process can be found in the Supporting Information). Thus, Ag cores from sample 1 with R_1 around 23 nm were prepared according to the standard sodium citrate reduction method,[30] whereas in sample 2, Ag cores of R_1 ca. 15 nm were synthesized via the polyol process (reduction in ethylene glycol at 120 °C in the presence of polyvinylpyrrolidone),[29] and for samples 3−6, Ag cores with R_1 between 6 and 9 nm were prepared via reduction with $NaBH_4$ using sodium citrate as capping agent.[31] The resulting Ag nanospheres were then coated with silica using modified procedures reported by Kobayashi et al.,[32] samples 1 and 3−6, and Graf et al.,[33] sample 2. The core−shell structure was characterized by transmission electron microscopy, revealing that, regardless of the sample, each single Ag nanoparticle was individually coated with a uniform silica shell (see Figure 1). The Ag core (R_1) and silica shell dimensions ($R_2 - R_1$, R_2 being the total radius) were determined from the analysis of TEM images. It should be noted that silica coating did not involve chemical binding of linker molecules

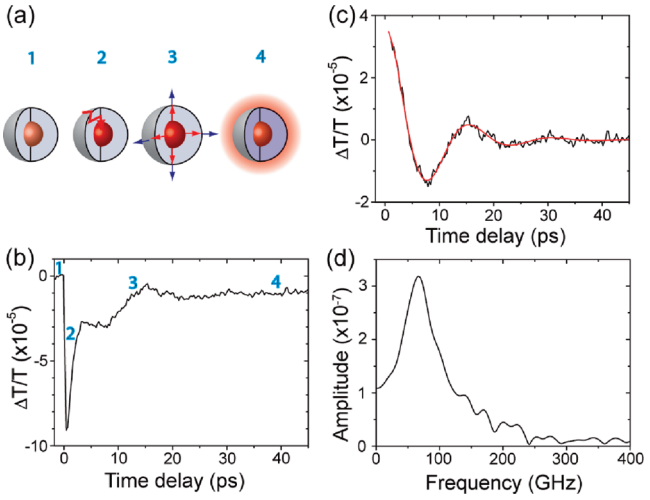

Figure 2. (a) Ultrafast excitation and time-dependent response of Ag@SiO_2 nanoparticles showing their initial configuration (1), heating of the metal core electrons by the pump pulse at time $t = 0$ and fast electron−lattice thermalization (2), launching of the core−shell vibration due to dilation of the heated core (3), and cooling of the particle due to energy transfer to the environment (4). (b) Probe transmission change $\Delta T/T$ measured in sample 1 as a function of pump−probe delay for pump and probe wavelengths of 850 and 425 nm, respectively. The processes described in (a) are indicated. (c) Oscillating part of $\Delta T/T$ (black signal) fitted with a damped sinusoid (red line) with period 15.3 ps and damping time 7.6 ps. (d) Fourier transform of the oscillating part of $\Delta T/T$, yielding a central frequency of 66 GHz (corresponding to a period of 15.2 ps).

between the silver cores and the grown silica shell, thus allowing mutual contact.

Optical experiments were performed using time-resolved pump−probe spectroscopy. A two-color pump−probe configuration adapted to excitation and detection of the acoustic vibration of metal nanoparticles[34] was used. In this technique, a first near-infrared femtosecond pump pulse excites the nanoparticles and a second time-delayed probe pulse follows the induced changes of the sample optical transmission $\Delta T/T$. Probing is performed around the wavelength λ_{SPR} of the surface plasmon resonance (SPR) of the particles to increase the probing sensitivity (with λ_{SPR} in the 400−430 nm range for our Ag@SiO_2 samples, see Figure 1c). The experimental setup is based on a homemade Ti:Sapphire oscillator delivering pulses of about 20 fs with a tunable wavelength around 850 nm at a repetition rate of 76 MHz. The output pulse train is split into two parts. The first is used to create the pump pulses, and the second is frequency-doubled in a 500 μm thick BBO crystal to generate the probe pulses. The two pulse trains are focused on the sample, and the delay t_D between pump and probe pulses is adjusted using a mechanical translation stage controlling the optical path of the probe beam. The pump beam is modulated at 100 kHz, and $\Delta T/T$ is measured using differential and lock-in detection of the pump-induced changes of probe beam transmission.

The pump−probe delay dependent $\Delta T/T$ signal measured in sample 1 (core radius $R_1 = (22.5 \pm 6.7)$ nm; shell thickness $R_2 - R_1 = (14.0 \pm 2.0)$ nm, see Table 1) is shown in Figure 2a,b for a probe wavelength $\lambda_{pr} = 425$ nm. As the pump pulse at 850 nm is only absorbed by the electrons of the Ag core, $\Delta T/T$ exhibits the usual temporal shape measured in silver nanoparticles around their SPR.[34,35] This signal is dominated by a ultrafast red shift of the SPR, which shows up by an induced transmission decrease

dx.doi.org/10.1021/nl201672k |Nano Lett. 2011, 11, 3016–3021

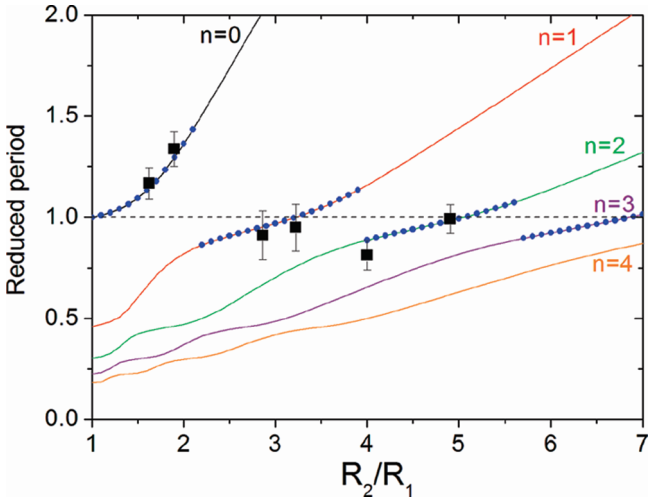

Figure 3. Reduced (i.e., divided by $T_{free}(R_1)$, see text) experimental periods measured in different samples as a function of the full over core radius R_2/R_1 (black squares, the sample number increases with R_2/R_1, Table 1). The reduced periods computed for the fundamental radial mode ($n = 0$) of an Ag@SiO_2 core−shell nanoparticle and for its four first harmonics ($n = 1-4$) are shown by the solid lines. The computed reduced period of the mode with largest amplitude in an optical pump−probe configuration is shown as blue dots. The black dashed line corresponds to the dominant reduced period expected in case of full core−shell decoupling (i.e., $T_{red}^{dom} = 1$).

when using a probe wavelength on the red side of the SPR ($\lambda_{SPR} \approx 420$ nm for sample 1). On a short time scale ($t_D \leq 3$ ps), this red shift reflects the heating of metal electrons and their subsequent cooling by energy transfer to the lattice (process 2 in Figure 2a) with a characteristic time constant of about 800 fs.[36] This fast electronic response is followed by pronounced oscillations overlapping with a slowly decaying (with a time constant of several hundred picoseconds) background signal. The latter reflects global cooling of the nanoparticles by energy transfer to the surrounding medium[37] (process 4 in Figure 2a) and will not be discussed here. The oscillating part of the signal is isolated by subtracting from the time-resolved $\Delta T/T$ two exponentially decaying contributions describing fast electron cooling kinetics and slow nanoparticle cooling. The resulting signal is shown in Figure 2c and, as for single material particles,[34] is well reproduced by a single damped sinusoidal function. This analysis yields an oscillation period $T_{osc} \approx 15.3$ ps, which is in excellent agreement with the frequency deduced from Fourier analysis (Figure 2d) and a damping time of 7.6 ps. Moreover, measurements performed on the same sample for different probe wavelengths around the SPR yield similar results.

Similarly to the case of single material particles, the temporal oscillations of $\Delta T/T$ are ascribed to acoustic vibrations of the core−shell particles (process 3 in Figure 2a). In the case of mono- or bimetallic nanospheres, temporal oscillations have been shown to be dominated by the nanosphere fundamental radial (breathing) mode.[15,38] In our Ag@SiO_2 particles, the measured period (15.3 ps, Figure 2c,d) is close to that of the breathing mode of the free core (about 13 ps for sample 1), but nevertheless deviates from it by about 20%. Similar results were achieved in the different investigated samples, and the measured oscillation periods T_{osc} are presented in Figure 3, as a function of the full particle over core size ratio, R_2/R_1 (Figure 1a). To facilitate comparison between samples, reduced periods obtained by dividing T_{osc} by the breathing mode period $T_{free}(R_1)$ of the bare core (i.e., of a free silver nanosphere of radius R_1) are shown. The error bars are estimated by comparing the outcome of different measurements/fitting procedures. Deviation of T_{osc} from T_{free} is observed for almost all samples, with a smaller amplitude for larger R_2/R_1 ratios. This convergence for large shell thicknesses is indeed expected, as T_{osc} should then be identical to the breathing mode period T_{mat} of Ag nanospheres in an infinite silica matrix, close to T_{free} ($T_{mat}(R_1) \approx 0.94\ T_{free}(R_1)$). The observed dependence of T_{osc} on R_2/R_1 indicates that the detected vibration modes involve motion in the whole particles, that is, both their metallic and dielectric parts vibrate (full decoupling conversely implying $T_{osc}/T_{free}(R_1) = 1$, black dashed line in Figure 3). This suggests a good mechanical contact of the core and shell, which is in contrast to previous results in dielectric-metal nanoparticles, where free vibration of the metal shell (showing mechanical decoupling of the core and shell) had been observed.[25,26]

More detailed analysis of the measured oscillations in the Ag@SiO_2 core−shell particles requires calculation of the vibrational modes of a full core−shell particle. For not too small particles, this can be performed using continuum mechanics together with the elastic properties of bulk materials.[19,20,34,39] Though this approach corresponds to size scaling the vibration of macroscopic objects, it is accurate for metal particles down to one nanometer sizes.[38] As a consequence of the isotropy of the excitation process in time-resolved experiments, only the radial modes of spherical nano-objects (i.e., characterized by a displacement field $\mathbf{u}(\mathbf{r},t) = u(r,t)\mathbf{u}_r$) can be excited. The characteristics of these modes have been computed in the case of monomaterial spheres either free[40] or embedded in an elastic[41] or viscoelastic[42] matrix. These models can be extended to the case of spherical core−shell or multiple shell nanoparticles.[20,25,28,43,44] Briefly, the displacements of the radial modes are solutions of the Navier equation in each considered j medium (i.e., core, shell or surrounding matrix)

$$\rho_j \frac{d^2 u_j}{dt^2} = (\lambda_j + 2\mu_j)\left[\frac{d^2 u_j}{dr^2} + \frac{2}{r}\frac{du_j}{dr} - \frac{2u_j}{r^2}\right] \quad (1)$$

where ρ_j is the density of the j region material, and λ_j and μ_j its Lamé constants. For a liquid matrix as investigated here, the above equation can be used assuming complex Lamé constants to take into account viscosity.[42] The eigenmodes are the harmonic solutions of eq 1: $u_j(r,t) = u_j(r)\exp(i\tilde{\omega}t)$ respecting the boundary conditions at the core−shell and shell−matrix interfaces, that is, continuity of the displacement and of the radial component of the stress tensor σ_{rr}. In the j layer, the latter is connected to $u_j(r,t)$ by

$$\sigma_{rr}^{j} = (\lambda_j + 2\mu_j)\frac{du_j}{dr} + 2\lambda_j \frac{u_j}{r} \quad (2)$$

For the relatively large nano-objects investigated here, displaying an external radius R_2 in the 21 to 37 nm range (Table 1), the presence of ethanol only weakly increases the mode periods as compared to the free particle ones (maximum by about 5%).[28] For the sake of simplicity, the ethanol environment will therefore be neglected here, that is, free particles will be assumed. The boundary condition at their outer interface thus corresponds to zero radial stress, $\sigma_{rr}^{shell}(R_2) = 0$ (with continuity of displacement and stress at the inner interface). The computed reduced periods of the vibrational radial modes only depend on the R_2/R_1 ratio and are shown in Figure 3 for the five first modes, labeled $n = 0$

dx.doi.org/10.1021/nl201672k |Nano Lett. 2011, 11, 3016–3021

to 4. They have been discussed in detail in ref 28. We just recall here that in the absence of an encapsulating shell ($R_2/R_1 = 1$), they correspond to the usual radial modes of a metal sphere. In the presence of a shell, displacement takes place in both the metal and dielectric parts, modifying vibrational periods. For each mode, period increases with R_2/R_1, reflecting evolution of the mode nature from that of the metal core to that of the shell (i.e., for large aspect ratios, the presence of the core becomes negligible).

The fact that a single mode dominates the time-resolved response of core−shell particles is a consequence of the optical excitation and detection processes.[28] In time-resolved experiments, the pump pulse selectively heats up the electrons of the metal core, which quickly transfer their energy to the core lattice. This creates a nonequilibrium situation with a hot core surrounded by a cold shell, which translates into a nonuniform thermal stress in the full core−shell particle. As a result, it evolves toward a new equilibrium configuration characterized by a larger size, which, as for single material nano-objects,[34] launches the particle vibration. The new equilibrium position can be computed using a thermoelasticity-based model, permitting us to define the initial radial displacement field (i.e., the difference between the core−shell particle configuration for a cold and hot metal core, i.e., before and after lattice heating by the pump pulse via the electrons).[28] The relative amplitudes of the excited modes imposed by the excitation process are thus obtained by projecting the initial displacement field on the orthogonal basis formed by the radial eigenmodes. Additionally, further mode selection takes place via the detection process. Indeed, the oscillating part of the probe pulse transmission reflects the modulation of the dielectric functions of the constituting materials imposed by their mechanical movement. For a transparent shell such as one made of silica, modulation of the dielectric function of the metal part yields the dominant contribution when probing in the optical domain. Assuming deformation potential coupling, this leads to an additional mode selection, where the corresponding weighting of each mode is proportional to the volume change induced in the core and can thus be computed from its associated displacement field.[28,45,46]

In time-resolved experiments, both the excitation and detection processes favor the modes involving large displacement in the core, which as expected correspond to periods close to the modes of the bare core. This is illustrated in Figure 4, which shows the amplitudes of the radial modes of largest periods computed for $R_2/R_1 = 1$, 1.5, and 5. In all cases, the mode with the closest period to the free core breathing mode period (i.e., with reduced period close to 1) is predicted to be preferentially observed. The order of the dominant mode in time-resolved measurements thus increases with R_2/R_1, corresponding to $n = 0$ for $R_2/R_1 = 1$ and 1.5 and to $n = 2$ for $R_2/R_1 = 5$. The computed reduced period T_{red}^{dom} of the dominant mode of the core−shell particle is shown in Figure 3 as a function of R_2/R_1 (blue dots). Its variation is in good agreement with the experimental results, which is in contrast to the constant reduced period ($T_{red}^{dom} = 1$) expected in the absence of contact at the metal-dielectric interface. This demonstrates that, conversely to previous experiments in dielectric core−metal shell particles, a good mechanical contact is achieved in our samples.

For shell thicknesses smaller than or of the order of the core radius, $R_2/R_1 \leq 2$, the fundamental radial mode of the full core−shell particle dominates the time-domain data. In this regime, increase of the shell thickness translates into an increase of the

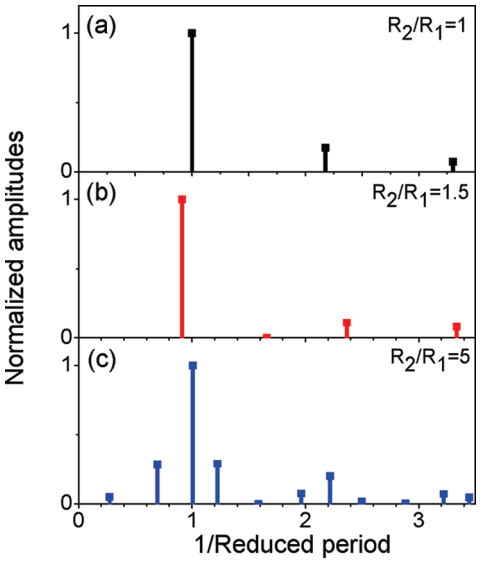

Figure 4. Computed amplitudes in time-resolved femtosecond experiments of the largest period radial modes of Ag@SiO_2 particles for (a) $R_2/R_1 = 1$ (modes $n = 0$ to 2), (b) $R_2/R_1 = 1.5$ (modes $n = 0$ to 3), and (c) $R_2/R_1 = 5$ (modes $n = 0$ to 10).

reduced period of the dominant mode, reflecting a contribution of the shell to the vibration. A maximum deviation of the mode period of about 45% from the bare core one is predicted for $R_2/R_1 \approx 2.1$, which is in excellent agreement with that measured for sample 2, about 35% for $R_2/R_1 \approx 1.9$. For larger silica shells, the mode with the largest amplitude is not anymore the fundamental one, but its harmonic with a reduced period close to 1 (blue dots in Figure 3). Over the investigated range, R_2/R_1 up to 5 (Table 1), the dominant mode switches from the fundamental one, $n = 0$, to its second harmonics, $n = 2$. Its reduced period T_{red}^{dom} thus first increases with increasing R_2/R_1, as it follows the period of the core−shell mode with index n, and jumps to a smaller value, as the dominant mode increments its order by 1. The amplitude of these variations decreases with increasing R_2/R_1 and, as expected, T_{red}^{dom} converges for large shells to the reduced period of the breathing mode of a silver nanosphere embedded in an infinite silica matrix $T_{red}^{dom} \approx 0.94$.

In the above theoretical model, free core−shell nanospheres have been assumed. This assumption is fully justified when computing vibrational periods, but obviously leads to no homogeneous damping (i.e., damping due to energy dissipation in the surrounding medium).[15,47] However, the model can be generalized to include damping in a viscoelastic matrix. These theoretical computations predict large dependences of the homogeneous damping rate of the dominant mode on both R_2/R_1 and the nature of the core−shell mechanical contact.[28] These effects cannot be observed here, since, as in most ensemble pump−probe measurements, vibrational damping is mostly of inhomogeneous nature, that is, mainly due to the progressive dephasing of the vibrations of the different nano-objects induced by their size and shape dispersions.[34,38] This is confirmed by the fact that an oscillation decay time of 7.5 ps is measured for sample 1, while a much longer homogeneous damping time of about 90 ps (due to energy dissipation in ethanol) is computed.

In conclusion, the acoustic vibrations of metal core−dielectric shell nanoparticles have been investigated using a time-resolved pump−probe technique. The results obtained as a function of

dx.doi.org/10.1021/nl201672k |*Nano Lett.* 2011, 11, 3016–3021

the relative shell and core sizes show that the presence of a dielectric shell significantly impacts the measured vibration frequencies. As the excitation and detection processes essentially involve the metal part of the core−shell particle, the observed vibration modes correspond to those with a maximum displacement in the metal core, that is, with a period close to the bare core breathing mode period. The measured vibration periods are in excellent agreement with those predicted by a theoretical model assuming perfect mechanical contact between the metal core and dielectric shell. The dependence of the period measured in time-resolved experiments on the core and shell size is a signature of this contact, yielding variation by up to about 40% around the breathing period of the core for a perfect contact and no variation for no contact. Optical investigation of the vibrational modes thus constitutes a unique tool for probing this contact at the nanoscale in nanohybrids. Extensions of this work to analyze the outcome of different synthesis methods of similar nanoparticles, or to study nano-objects with other shapes or structure (multiple metal/dielectric components) would be particularly interesting. Moreover, whereas our study focused on vibrational periods, the vibrational damping of core−shell nanoparticles also contains important information on its characteristics. However, addressing this process is much more difficult, since except in some cases,[15,47] it requires experiments on single nanoparticles[48−50] to avoid spurious effects due to inhomogeneous damping.

■ ASSOCIATED CONTENT

Supporting Information. Additional information about nanoparticle synthesis is available. This material is available free of charge via the Internet at http://pubs.acs.org.

■ AUTHOR INFORMATION

Corresponding Author
*E-mail: pmaioli@lasim.univ-lyon1.fr.

■ ACKNOWLEDGMENT

N.D.F. acknowledges support by the Institut Universitaire de France (IUF). This work was funded by the "Opthermal" Grant of the Agence Nationale de la Recherche and by the France-Spain PHC Picasso program (Acciones Integradas MICINN, FR2009-0034). L.M.L.-M. acknowledges support from the Xunta de Galicia (Grant #09TMT011314PR).

■ REFERENCES

(1) Mokari, T.; Rothenberg, E.; Popov, I.; Costi, R.; Banin, U. *Science* **2004**, *304*, 1787.
(2) Majimel, J.; Bacinello, D.; Durand, E.; Vallée, F.; Treguer-Delapierre, M. *Langmuir* **2008**, *24*, 4289.
(3) Jackson, J. B.; Halas, N. J. *J. Phys. Chem. B* **2001**, *105*, 2743.
(4) Prodan, E.; Radloff, C.; Halas, N. J.; Nordlander, P. *Science* **2003**, *302*, 419.
(5) Rodriguez-Fernandez, J.; Pastoriza-Santos, I.; Perez-Juste, J.; Garcia de Abajo, F. J.; Liz-Marzan, L. M. *J. Phys. Chem. C* **2007**, *111*, 13361.
(6) Liz-Marzan, L. M.; Giersig, M.; Mulvaney, P. *Langmuir* **1996**, *12*, 4329.
(7) Sershen, S. R.; Westcott, S. L.; West, J. L.; Halas, N. J. *Appl. Phys. B* **2001**, *73*, 379.
(8) Loo, C.; Lowery, A.; Halas, N. J.; West, J.; Drezek, R. *Nano Lett.* **2005**, *5*, 709.
(9) O'Neal, D. P.; Hirsch, L. R.; Halas, N. J.; Payne, J. D.; West, J. L. *Cancer Lett.* **2004**, *209*, 171.
(10) Gobin, A. M.; Lee, M. H.; Halas, N. J.; James, W. D.; Drezek, R. A.; West, J. L. *Nano Lett.* **2007**, *7*, 1929.
(11) Muskens, O. L.; Billaud, P.; Broyer, M.; Del Fatti, N.; Vallée, F. *Phys. Rev. B* **2008**, *78*, 205410.
(12) Muskens, O. L.; Bachelier, G.; Del Fatti, N.; Vallée, F.; Brioude, A.; Jiang, X. C.; Pileni, M. P. *J. Phys. Chem. C* **2008**, *112*, 8917.
(13) Kelly, K. L.; Coronado, E.; Zhao, L. L.; Schatz, G. C. *J. Phys. Chem. B* **2003**, *107*, 668.
(14) Hodak, J. H.; Martini, I.; Hartland, G. V. *J. Chem. Phys.* **1998**, *108*, 9210.
(15) Del Fatti, N.; Voisin, C.; Chevy, F.; Vallée, F.; Flytzanis, C. *J. Chem. Phys.* **1999**, *110*, 11484.
(16) Juvé, V.; Crut, A.; Maioli, P.; Pellarin, M.; Broyer, M.; Del Fatti, N.; Vallée, F. *Nano Lett.* **2010**, *10*, 1853.
(17) Hu, M.; Wang, X.; Hartland, G. V.; Mulvaney, P.; Juste, J. P.; Sader, J. E. *J. Am. Chem. Soc.* **2003**, *125*, 14925.
(18) Hu, M.; Hillyard, P.; Hartland, G. V.; Kosel, T.; Perez-Juste, J.; Mulvaney, P. *Nano Lett.* **2004**, *4*, 2493.
(19) Crut, A.; Maioli, P.; Del Fatti, N.; Vallée, F. *Phys. Chem. Chem. Phys.* **2009**, *11*, 5882.
(20) Sader, J. E.; Hartland, G. V.; Mulvaney, P. *J. Phys. Chem. B* **2002**, *106*, 1399.
(21) Portales, H.; Goubet, N.; Saviot, L.; Adichtchev, S.; Murray, D. B.; Mermet, A.; Duval, E.; Pileni, M. P. *Proc. Natl. Acad. Sci. U.S.A.* **2008**, *105*, 14784.
(22) Zijlstra, P.; Tchebotareva, A. L.; Chon, J. W. M.; Gu, M.; Orrit, M. *Nano Lett.* **2008**, *8*, 3493.
(23) Portales, H.; Goubet, N.; Saviot, L.; Yang, P.; Sirotkin, S.; Duval, E.; Mermet, A.; Pileni, M. P. *ACS Nano* **2010**, *4*, 3489.
(24) Voisin, C.; Christofilos, D.; Del Fatti, N.; Vallée, F. *Physica B* **2002**, *316*, 89.
(25) Guillon, C.; Langot, P.; Del Fatti, N.; Vallée, F.; Kirakosyan, A. S.; Shahbazyan, T. V.; Cardinal, T.; Treguer, M. *Nano Lett.* **2007**, *7*, 138.
(26) Mazurenko, D. A.; Shan, X.; Stiefelhagen, J. C. P.; Graf, C. M.; van Blaaderen, A.; Dijkhuis, J. I. *Phys. Rev. B* **2007**, *75*, 161102.
(27) Portales, H.; Saviot, L.; Duval, E.; Gaudry, M.; Cottancin, E.; Pellarin, M.; Lermé, J.; Broyer, M. *Phys. Rev. B* **2002**, *65*, 165422.
(28) Crut, A.; Juvé, V.; Mongin, D.; Maioli, P.; Del Fatti, N.; Vallée, F. *Phys. Rev. B* **2011**, *83*, 205430.
(29) Silvert, P. Y.; HerreraUrbina, R.; Duvauchelle, N.; Vijayakrishnan, V.; Elhsissen, K. T. *J. Mater. Chem.* **1996**, *6*, 573.
(30) Turkevich, J.; Stevenson, P. C.; Hillier, J. *Discuss. Faraday Soc.* **1951**, 55.
(31) Ung, T.; Liz-Marzan, L. M.; Mulvaney, P. *Langmuir* **1998**, *14*, 3740.
(32) Kobayashi, Y.; Katakami, H.; Mine, E.; Nagao, D.; Konno, M.; Liz-Marzan, L. M. *J. Colloid Interface Sci.* **2005**, *283*, 392.
(33) Graf, C.; Vossen, D. L. J.; Imhof, A.; van Blaaderen, A. *Langmuir* **2003**, *19*, 6693.
(34) Voisin, C.; Del Fatti, N.; Christofilos, D.; Vallée, F. *J. Phys. Chem. B* **2001**, *105*, 2264.
(35) Del Fatti, N.; Voisin, C.; Achermann, M.; Tzortzakis, S.; Christofilos, D.; Vallée, F. *Phys. Rev. B* **2000**, *61*, 16956.
(36) Arbouet, A.; Voisin, C.; Christofilos, D.; Langot, P.; Del Fatti, N.; Vallée, F.; Lermé, J.; Celep, G.; Cottancin, E.; Gaudry, M.; Pellarin, M.; Broyer, M.; Maillard, M.; Pileni, M. P.; Treguer, M. *Phys. Rev. Lett.* **2003**, *90*, 177401.
(37) Juvé, V.; Scardamaglia, M.; Maioli, P.; Crut, A.; Merabia, S.; Joly, L.; Del Fatti, N.; Vallée, F. *Phys. Rev. B* **2009**, *80*, 195406.
(38) Hartland, G. V. *Annu. Rev. Phys. Chem.* **2006**, *57*, 403.
(39) Hartland, G. V. *J. Chem. Phys.* **2002**, *116*, 8048.
(40) Lamb, H. *Proc. London Math. Soc.* **1882**, *13*, 189.
(41) Dubrovskiy, V. A.; Morochnik, V. S. *Earth Phys.* **1981**, *17*, 494.
(42) Saviot, L.; Netting, C. H.; Murray, D. B. *J. Phys. Chem. B* **2007**, *111*, 7457.

(43) Kirakosyan, A. S.; Shahbazyan, T. V. *Appl. Phys. B* **2006**, *84*, 117.
(44) Kirakosyan, A. S.; Shahbazyan, T. V. *J. Chem. Phys.* **2008**, *129*, 034708.
(45) Arbouet, A.; Del Fatti, N.; Vallée, F. *J. Chem. Phys.* **2006**, *124*, 144701.
(46) Nelet, A.; Crut, A.; Arbouet, A.; Del Fatti, N.; Vallée, F.; Portales, H.; Saviot, L.; Duval, E. *Appl. Surf. Sci.* **2004**, *226*, 209.
(47) Pelton, M.; Sader, J. E.; Burgin, J.; Liu, M. Z.; Guyot-Sionnest, P.; Gosztola, D. *Nat. Nanotechnol.* **2009**, *4*, 492.
(48) Burgin, J.; Langot, P.; Del Fatti, N.; Vallée, F.; Huang, W.; El-Sayed, M. A. *J. Phys. Chem. C* **2008**, *112*, 11231.
(49) Muskens, O. L.; Del Fatti, N.; Vallée, F. *Nano Lett.* **2006**, *6*, 552.
(50) Baida, H.; Christofilos, D.; Maioli, P.; Crut, A.; Del Fatti, N.; Vallée, F. *J. Raman Spectrosc.* **2011**10.1002/jrs.2874.